Analysis of tunnels in shaly rock considering three-dimensional stress effects on swelling

B.C. Hawlader, K.Y. Lo, and I.D. Moore

Abstract: Underground structures in shales or shaly rocks endure time-dependent swelling effects. Laboratory test results show that the swelling of these shales is dependent on three-dimensional stresses; an external stress on a specimen in one principal direction reduces the swelling not only in that direction but also perpendicularly. The effectiveness of a time-dependent swelling model that considers the three-dimensional stress effect is presented in this paper. A finite element algorithm incorporating the new constitutive model is used for a numerical analysis. The finite element program is used to analyze two tunnels in southern Ontario: the Heart Lake storm sewer tunnel, and the Darlington cold-water intake tunnel. The predicted results agree well with the records of field performance of these tunnels. The comparison between present analyses and the existing closed-form solution shows that the existing solution overestimates the time-dependent swelling effects. The three-dimensional stress effects on swelling are not considered in the closed-form solutions and are the cause of this discrepancy. The pseudo-Poisson's effect is a key parameter for modelling the observed time-dependent swelling. The use of these solutions in design is discussed.

Key words: time-dependent swelling, shale, modelling, three-dimensional stress effect, finite element method, tunnel.

Résumé : Les structures souterraines dans les shales et les roches schisteuses subissent des effets de gonflement en fonction du temps. Les résultat d'essais en laboratoire montrent que le gonflement de ces shales dépend des contraintes tridimensionnelles ; une contrainte extérieure sur un spécimen dans une direction principale réduit le gonflement non seulement dans cette direction mais aussi perpendiculairement. Dans cet article, on présente l'efficacité d'un modèle de gonflement en fonction du temps qui tient compte de l'effet des contraintes tridimensionnelles. On utilise un algorithme en éléments finis incorporant le nouveau modèle constitutif pour une analyse numérique. Le programme en éléments finis est utilisé pour analyser deux tunnels dans le sud de l'Ontario : le Heart Lake storm sewer tunnel et le Darlington cold-water intake tunnel. Les résultats prédits concordent bien avec les données de la performance sur le terrain. La comparaison entre ces présentes analyses et la solution exacte existante montre que la solution existante surestime les effets de gonflement en fonction du temps. Les effets de la contrainte tridimensionnelle sur le gonflement ne sont pas prises en compte dans les solutions exactes et sont la cause de cette divergence. Le pseudo-effet de Poisson est un paramètre clé pour modéliser le gonflement observé en fonction du temps. On discute de l'utilisation de ces solutions dans la conception.

Mots clés : gonflement en fonction du temps, shale, modélisation, effet des contraintes en trois dimensions, méthode des éléments finis, tunnel.

[Traduit par la Rédaction]

Introduction

Numerous tunnels have been built and new tunnels are planned for construction in the shales and shaly rocks in southern Ontario. Case studies (e.g., Lo et al. 1978; Lo and Yuen 1981; Lo 1986) show that underground structures built

B.C. Hawlader. C-CORE, Morrissey Road, St. John's, NL A1B 3X5, Canada.
K.Y. Lo.[1] Geotechnical Research Centre, Faculty of Engineering, University of Western Ontario, London, ON N6A 5B9, Canada.
I.D. Moore. Infrastructure Engineering, Queen's University, Kingston, ON K7L 3N6, Canada.

[1]Corresponding author (e-mail: kylo@uwo.ca).

in these formations have undergone stress-dependent long-term swelling deformation (Lo et al. 1978). Lo and Lee (1990) show in laboratory tests that the application of stress on a rock specimen reduces the swelling strain not only in the direction of applied stress but also in its orthogonal directions. As an example, a relatively small amount of vertical stress (~ 0.02 MPa) reduces the free swell potential by 30% in the horizontal direction where no external stresses are applied. The swelling deformation is anisotropic due to the inherent rock structure (e.g., the free swell potential of Georgian Bay shale in the vertical direction is three to five times that in the horizontal direction within the 2%–6% range of calcite content; Lo et al. 1979). Moreover, these shales are typically in a highly anisotropic in situ stress state, with the horizontal stress much higher than the vertical stress (e.g., initial stress ratio $K_0 = 10$ for the rock formation around the Darlington cold-water intake tunnel; Lo and Lukajic 1984). Therefore, it is necessary to analyze the time-

Fig. 1. Inward movement of the wheelpit at Niagara Falls (after Lee and Lo 1976).
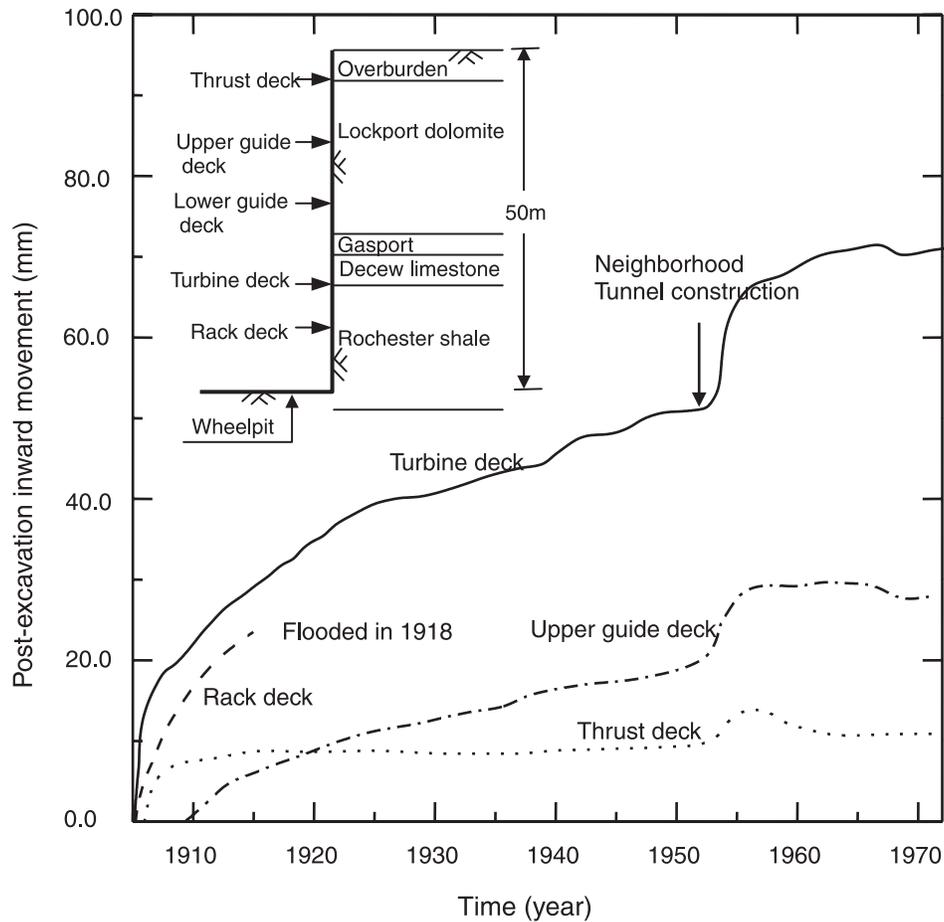
dependent swelling behaviour under three-dimensional stress conditions for the design of tunnels.

Based on the so-called "swelling law," several time-independent constitutive models are developed for the swelling of rocks (e.g., Grob 1972; Einstein et al. 1972; Wittke and Pierau 1979). These models are not appropriate for the shales in southern Ontario, as the swelling of these shales is due to moisture migration rather than chemical changes (Lee and Lo 1993). The International Society of Rock Mechanics (ISRM Commission on Swelling Rock 1994) examined the swelling models available in the literature and concluded that, although the swelling deformation due to chemical change may be adequately predicted using available models, time-dependent swelling models need to be developed from a fundamental knowledge of the swelling mechanism. Lo and Yuen (1981) and Lo and Hefny (1996) have developed rheological models for the time-dependent swelling of rocks. Closed-form solutions developed in both studies predict the swelling effects on a circular tunnel. Field performance of the existing tunnels shows that these models simulate the trend of swelling behaviour very well, and the models are used in the design of several underground structures in southern Ontario (e.g., Lo et al. 1986; Trow and Lo 1989). Lo and Yuen (1981) did not consider any stress effect on swelling in their model, and Lo and Hefny (1996) assumed that only the radial pressure on the lining affects the swelling deformation. As shown in the paper, the omission of any

stress effect makes the prediction conservative. It is also necessary to predict the long-term swelling deformation that is observed in the field. As an example, the swelling deformation of a wheelpit at Niagara Falls (Lee and Lo 1976) is shown in Fig. 1 where the time-dependent deformation for 75 years has been recorded. Hawlader et al. (2003) have developed a constitutive model for the swelling of rock that considers the three-dimensional stress effects and anisotropic swelling. The anisotropic and three-dimensional stress-dependent swelling model cannot be accommodated in a closed-from solution, and a numerical solution must be employed.

The main objective of this paper is to develop a numerical approach to study swelling effects on underground structures. The paper consists of three parts. The first part briefly describes the swelling model that has been developed from the laboratory test results on the shales in southern Ontario. The second part deals with the model implementation in a finite element code. Lastly, the numerical code is used to analyze the case histories of the Heart Lake storm sewer tunnel (Lo et al. 1979; Lo and Yuen 1981) and the Darlington cold-water intake tunnel (Lo and Lukajic 1984).

Swelling model

Laboratory tests on shales in southern Ontario (e.g., Lo and Lee 1990) show that the swelling strains in the principal

directions of a rock specimen increase linearly with the logarithm of time. The slope of this line is denoted as the "swelling potential" (Lo et al. 1978). Maximum swelling occurs when there is zero external pressure acting on the specimen. The swelling potential under zero external pressure is known as the "free swelling potential." The swelling potential decreases with increases in applied stress on the specimen. The stress in one principal direction reduces the swelling strain not only in that direction but also perpendicularly (Lo and Lee 1990). Hawlader et al. (2003) modelled the swelling of rock under three-dimensional stress using the following set of equations:

[1] $\varepsilon_i^s(t) = m_i \log(t/t_0)$

[2] $m_i = (1 - R_i^{TS}) m_{i(0)}$

[3] $R_i^{TS} = \dfrac{\log(\sigma_i^{TS}/\sigma_{th})}{\log(\sigma_c/\sigma_{th})}$

[4] $\sigma_i^{TS} = \sigma_i + (1 - \delta_{ij}) \sigma_{th} 10^{[R_{ij} \log(\sigma_c/\sigma_{th})]}$

[5] $R_{ij} = \mu_{ij} R_{jj}$

[6] $R_{jj} = \dfrac{\log(\sigma_j/\sigma_{th})}{\log(\sigma_c/\sigma_{th})}$

where $\varepsilon_i^s(t)$ is the swelling strain in the ith principal direction at time t; m_i is the swelling potential under the three-dimensional stress condition; δ_{ij} is the Kronecker delta; t_0 is the reference time; R_{ij} are the reduction ratios; and the superscripts i and j represent the principal directions.

The input parameters required for this model are (*i*) free swelling potential ($m_{i(0)}$); (*ii*) threshold stress (σ_{th}), where the stress below which applied stress has no effect on swelling; (*iii*) critical stress (σ_c), where stress equal to or greater than this magnitude completely suppresses swelling; (*iv*) pseudo-Poisson's ratio (μ); and (*v*) reference time (t_0), which is the time from which swelling begins. The first four input parameters can be obtained from free swell and modified semi-confined swell tests (Lee 1988; Hawlader et al. 2003), and t_0 can be obtained from the expected advance rate of the tunnel during construction. Further details are discussed in the following sections.

The main objective of this paper is the implementation of the aforementioned model in the numerical analysis. The physical aspects of the model can be found in Hawlader et al. (2003).

Swelling effects on tunnels

The model described in the previous section is used to predict the swelling effects on underground structures. Consider a tunnel in a swelling rock mass as shown in Fig. 2*a*. The horizontal and vertical axes are represented by x and y, respectively, and r and θ represent the radial and angular positions of a rock element, respectively. The in situ stress components of a rock element are σ_{x0} and σ_{y0} and are shown in Fig. 2*b* after excavation at a point A. The stress effect on swelling modelled in the section titled Swelling model is in the principal axis system. Figure 2*c* shows the transformed stresses in the principal directions. The direction of the major principal stress relative to the horizontal axis (x) is repre-

sented by an angle α_{p1} (Fig. 2*c*). The free swelling potentials are shown in Fig. 2*d*, which shows that the free swelling potential is different in the horizontal and vertical directions in the anisotropic swelling model and is constant for the isotropic swelling model.

Three-dimensional stress change occurs near the face of the tunnel during the excavation. Lo and Lukajic (1984) show that, once the tunnel face advances to a distance of three times its equivalent radius (r_e), the three-dimensional condition approaches a state of plane strain and the elastic changes of stress and displacement are essentially completed. Independent measurement of deformation caused by elastic stress change or swelling is not possible in this zone. Therefore, it is assumed that the deformation in this zone is purely elastic. The time required for this is used as the reference time, t_0, in the field (Fig. 2*e*). The time-dependent swelling deformation is modelled as beginning from this time. For design calculations (Lo and Lukajic 1984), the tunnel is unlined for a time t_l (Fig. 2*e*) before the lining is installed. A substantial amount of swelling deformation occurs during this time which reduces the subsequent development of lining stress due to swelling of the rock. The time lapse after installation of the lining is represented by t' ($= t - t_l$).

Constitutive equations

The total strain consists of elastic (denoted by the superscript "e" in the following sections) and swelling (denoted by the superscript "s") components. The strain components in incremental form can be written as

[7] $\dot{\boldsymbol{\varepsilon}} = \dot{\boldsymbol{\varepsilon}}^e + \dot{\boldsymbol{\varepsilon}}^s$

The elastic strain increment ($\dot{\boldsymbol{\varepsilon}}^e$) is related to the stress increment ($\dot{\boldsymbol{\sigma}}$) as

[8] $\dot{\boldsymbol{\sigma}} = \mathbf{D} \dot{\boldsymbol{\varepsilon}}^e$

where the fourth-order tensor $\mathbf{D}$ is the elasticity matrix given by

[9] $\mathbf{D} = \dfrac{E}{2(1+\nu)} \left[\dfrac{2\nu}{1-2\nu} \delta_{ij}\delta_{kl} + \delta_{ik}\delta_{jl} + \delta_{il}\delta_{jk} \right]$

for elastic modulus (E) and Poisson's ratio (ν).

The swelling strain rate in the principal direction ($\dot{\varepsilon}_p^s$) is related to the swelling potential as (differentiating eq. [1])

[10] $\dot{\varepsilon}_p^s = 0.434 \, m/t$

where the subscript "p" is used to represent the principal directions of a rock element in the field. The swelling potential (m) under the three-dimensional stress condition can be obtained from eq. [2].

Numerical algorithm

As shown in previous sections, the swelling deformation of rock is nonlinear and stress dependent. The incremental finite element approach (Zienkiewicz and Taylor 1990) is used to solve this problem. The explicit integration method (or initial strain approach; Zienkiewicz and Cormeau 1974) is used to implement the present model in a general purpose

Fig. 2. (*a*) Sign convention and geometry. (*b*) Stress components at point A after excavation. (*c*) Principal stress components at point A. (*d*) Free swell potentials. (*e*) Definition of time.

(a)

(b)

(c)

(d)

(e)
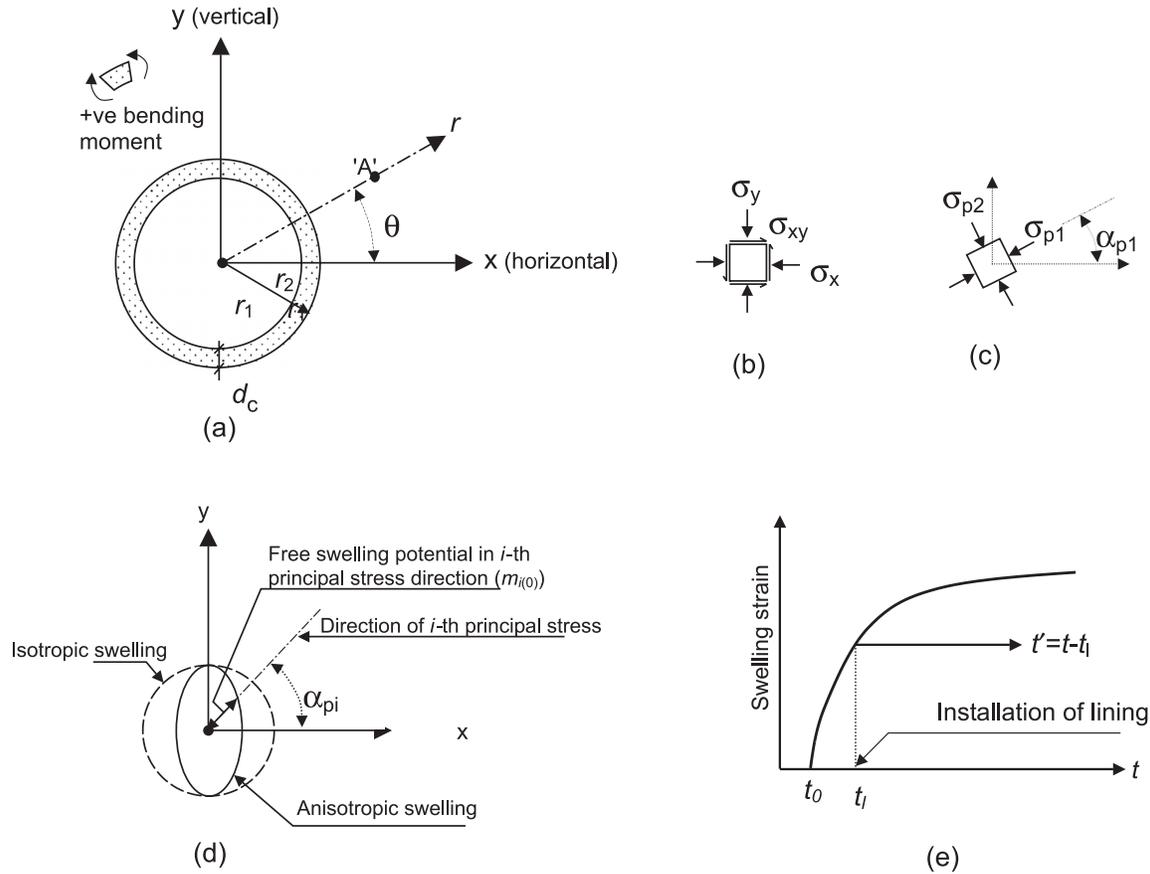
finite element program called AFENA (Carter and Balaam 1990).

As is common in the finite element analysis, the formulation uses the principle of virtual work. According to the initial strain approach, the equilibrium equations, compatibility conditions, and stress–strain relations for the *n*th time step are represented as

[11] $\mathbf{K}\Delta a^n = \Delta F^{*n} + \Delta F^n_{\text{ext}} + F^{n-1}_{\text{ext}} - F^{n-1}_{\text{int}}$

[12] $\Delta \varepsilon^n = \mathbf{B}\Delta a^n$

[13] $\Delta \sigma^n = \mathbf{D}[\Delta \varepsilon^n - (\Delta \varepsilon^s)^n]$

with

[14] $\mathbf{K} = \int_\Omega \mathbf{B}^T \mathbf{D} \mathbf{B} d\Omega$

[15] $\Delta F^{*n} = \int_\Omega \mathbf{B}^T \mathbf{D}(\Delta \varepsilon^s)^n d\Omega$

[16] $F^{n-1}_{\text{int}} = \int_\Omega \mathbf{B}^T \sigma^{n-1} d\Omega$

where $\mathbf{K}$ is the stiffness matrix of the element assemblage; ΔF^{*n} is the pseudo-load vector increment; ΔF^n_{ext} is the external load vector increment; F^{n-1}_{ext} and F^{n-1}_{int} are the external and internal force vectors, respectively; the superscripts *n* and *n* – 1 are used to represent time step *n* and its predeces-

sor; *a* is the nodal displacement vector; matrix $\mathbf{B}$ relates strain and displacement using shape functions; σ and ε are the stress and strain vectors, respectively; and Ω is the volume of the body. The difference between external and internal force vectors ($F^{n-1}_{\text{ext}} - F^{n-1}_{\text{int}}$) is the unbalanced or residual force vector due to truncation and round-off error. Ideally, it should vanish at the end of each step, but for a nonlinear analysis 100% equilibrium seldom occurs. The use of this force in eq. [11] avoids the accumulation of errors and ensures the total equilibrium of the solution.

Step-by-step procedure

The formulation described in the previous section requires step-by-step computation. The excavation of the tunnel is considered an instant unloading that corresponds to the elastic calculation step. There is no change in external load in the following time steps ($\Delta t^n = t^n - t^{n-1}$). The time-dependent swelling deformation occurs at this stage and causes the redistribution of internal stresses. The plane strain condition is used in the analysis, and the algorithm used to move from the (*n* – 1)th to *n*th time step is as follows:

(1) The calculation begins with the values of σ^{n-1}, ε^{n-1}, a^{n-1}, and F^{n-1} at the (*n* – 1)th time step. Determine the incremental external load vector (ΔF^n_{ext}), and calculate the internal force vectors (F^{n-1}_{int}) and pseudo-load vector (ΔF^{*n}) using eqs. [16] and [15], respectively.

(2) Calculate the incremental displacement vector (Δa^n) using eq. [11], and find the strain increment vector ($\Delta \varepsilon^n$) using the strain–displacement relationship given in eq. [12].

(3) Calculate the magnitudes (σ_p^{n-1}) and rotations (α_p^{n-1}) of the principal stresses (Fig. 2c) from σ^{n-1}, and then calculate the free swelling potentials in the principal stress directions as (Fig. 2d)

[17] $\quad m_{i(0)} = m_{x(0)} \cos \alpha_{pi} + m_{y(0)} \sin \alpha_{pi}$

where $i = 1$ and 2 for the major and minor principal stresses, respectively.

(4) Calculate the reduction ratios in the principal stress directions (R_{jj}) and in the orthogonal directions (R_{ij}) using eqs. [6] and [5], respectively.

(5) Calculate the total suppression stress (σ_i^{TS}) using eq. [4].

(6) Calculate R_i^{TS} using eq. [3], and then from eq. [2] calculate the swelling potentials (m_i) under the three-dimensional stress state.

(7) Compute the swelling strain rates ($\dot{\varepsilon}_p^s$) in the principal directions using eq. [10] and transfer them to $\dot{\varepsilon}^s$ in the (x, y, z) coordinate system.

(8) Determine the incremental swelling strain ($\Delta \varepsilon^s$) within the nth time step:

[18] $\quad (\Delta \varepsilon^s)^n \approx (\dot{\varepsilon}^s)^{n-1} \Delta t$

(9) Calculate the stress increment ($\Delta \sigma^n$) using eq. [13].

(10) Update the stress, strain, and displacement at the end of the nth time step; these are the starting values of the next time step:

$$\sigma^n = \sigma^{n-1} + \Delta \sigma^n$$
[19] $\quad \varepsilon^n = \varepsilon^{n-1} + \Delta \varepsilon^n$
$$a^n = a^{n-1} + \Delta a^n$$

The computation is then shifted to the next time step and the process is repeated until the assigned time is completed. Note that the deformation behaviour of the rock is modelled with nonlinear swelling over time and provides an instantaneous response based on linear elasticity. The main advantage in using the initial strain approach is that the stiffness matrix is only assembled and disassembled at the very beginning of the computation and is used in all iterations. The swelling effects are incorporated using the pseudo-load vector (eq. [15]).

All analyses presented here employ a finite element mesh using six-noded triangular plane strain elements for the rock and straight beam–column elements for the concrete lining. A no-slip (perfectly rough) condition is assumed for the rock–lining interface. The lining is considered to be elastic. The swelling strain rate is higher for the rock elements near the excavation because of the higher stress reductions. Therefore, smaller elements are used near the face of the excavation and the element size is increased with an increase in the radial distance. The swelling deformation is nonlinear, with a greater magnitude at the beginning of the calculation (see eq. [1]). An initial time step of 0.1 days is used in the analyses and is gradually increased to 2 days after 10 years of swelling. These time steps maintain the numerical stability that is an important issue in time-dependent analysis.

Application of the model to case records

The numerical procedure in the previous section is used to analyze two tunnels in swelling rocks in southern Ontario. The performance of these tunnels is monitored over a long period of time (Lo and Yuen 1981; Lo and Lukajic 1984).

Heart Lake tunnel

Heart Lake tunnel is a trunk storm sewer tunnel constructed in 1975 near the Pearson International Airport, Toronto. The tunnel is 3 m in finished diameter and 1.5 km long. Three construction methods were used: (i) cut and cover (232 m), (ii) drill and blast (183 m), and (iii) machine boring (1050 m). Lo and his coworkers (Lo et al. 1979; Lo and Yuen 1981) reported the geological conditions of the site and the properties of the rock. The in situ stress condition and the properties of the rock and lining used in this analysis are obtained from those works and are listed in Table 1. The numerical analyses are mainly performed for a machine-bored section at CH 136+20 (Fig. 12 of Lo and Yuen 1981). This section is considered for two reasons: (i) the in situ horizontal stresses around the section were measured (Lo et al. 1979), and (ii) the rock around the machine-bored section is relatively intact compared to the drill and blast section where the rock is fractured due to blasting. It is shown later that higher values of K_0 lead to greater lining stress as a result of swelling. A parametric study is also performed for K_0 because the lateral earth pressure coefficient decreases towards the upstream direction.

The change in initial stress caused by the excavation initiates the time-dependent swelling deformation of the rock (Lo 1978). Analysis and field measurement (Lo et al. 1979) show that the in situ stress change due to excavation is very small beyond a radial distance of $5r_2$, where r_2 is the radius of excavation. As the depth of the tunnel at CH 136+20 is considerably greater than this, the tunnel is considered to be "deep," so only one quarter of the tunnel section needs to be analyzed.

As mentioned earlier, the swelling deformation of rock is modelled to begin when the tunnel face advances to a distance of three times the equivalent radius (r_e). Numerical analyses show that the difference between the predicted lining stresses using t_0 values equal to 5 and 20 days is only 5% after 3 years of swelling. Moreover, the difference reduces with time. As long-term effects are the main concern in the design for swelling, any selection of t_0 within this range of time is suitable for design. The values of t_0 for the following calculations have been selected from the excavation records of the tunnel during construction.

Results of analysis

Once the lining is in contact with rock, the time-dependent swelling of the surrounding rock generates axial thrust and bending moment within it. The non-uniform swelling of rock under anisotropic stress distribution causes the bending moment. A value of 12 for the initial stress ratio ($K_0 = \sigma_{x0}/\sigma_{y0}$) is used in this analysis (Lo and Yuen 1981). The development of the axial thrust in the concrete lining is shown in Fig. 3. The axial thrust is mainly compressive and is maximum at the crown. The distribution of the bending moment in the concrete lining is shown in Fig. 4. The bend-

Table 1. Geometry and parameters used in the analyses.

	Heart Lake	Darlington
Geometry		
Outer radius of tunnel, r_2 (m)	1.675	4.5
Thickness of concrete lining, d_c (m)	0.3	0.5
Shape of the tunnel	Circular	D-shaped
Initial stress		
Vertical stress, σ_{y0} (MPa)	0.435	Overburden
Horizontal stress, σ_{x0}	$K_0\sigma_{y0}$	Field (Fig. 11)
Rock properties		
Elastic		
Elastic modulus, E_r (MPa)	12 400	25 000
Poisson's ratio, ν_r	0.15	0.33
Time-dependent swelling		
Threshold stress, σ_{th} (MPa)	0.001	0.001
Ratio of critical stress to horizontal stress, σ_c/σ_{x0}	0.6	0.6
Reference time, t_0 (days)	10	10
Pseudo-Poisson's ratio, μ	0.6	0.6
Free swelling potentials (%)		
$m_{x(0)}$	0.10	0.025
$m_{y(0)}$	0.42	0.060
$m_{z(0)}$	0.10	0.025
Concrete lining		
Elastic modulus, E_l (MPa)	28 000	28 000
Poisson's ratio, ν_l	0.2	0.2
Time of lining installation, t_l (days)	100	100

Fig. 3. Development of axial thrust in the concrete lining with time (Heart Lake tunnel) (positive compression).

Fig. 4. Development of bending moment in the concrete lining (Heart Lake tunnel). Positive moment causes tensile stress at the inner face.
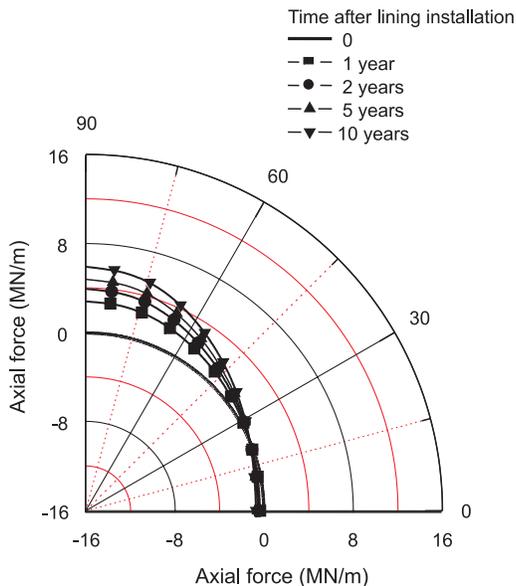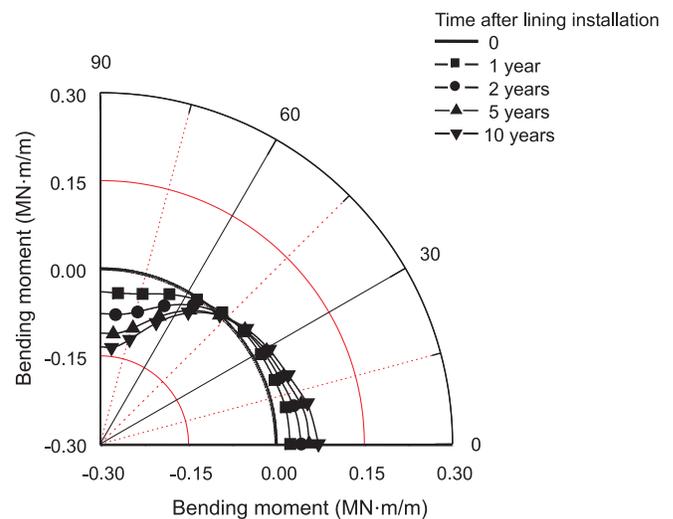
ing moment is positive at the springline, gradually decreasing to zero at $\theta \approx 50°$ and becoming negative at the crown. The sign convention used here is a positive bending moment that causes tensile stress at the inner fibre of the concrete lining. The axial thrust and bending moment distributions show that the maximum stresses in tension and compression occur at the inner face of the lining at the springline and crown, respectively. Therefore, discussion in the following sections focuses mainly on the stresses at the inner face of the lining.

Figure 5 shows the tangential stress at the inner face of the lining, which is tensile (negative) at the springline and compressive (positive) at the crown. The magnitude of stress

Fig. 5. Development of tangential stress at the inner surface of the lining (Heart Lake tunnel; positive compression).
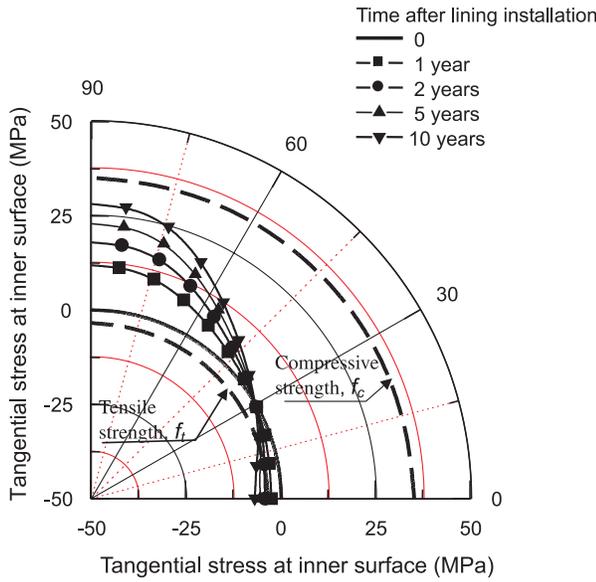
Fig. 6. Predicted radial displacement of Heart Lake tunnel with time (negative inward).
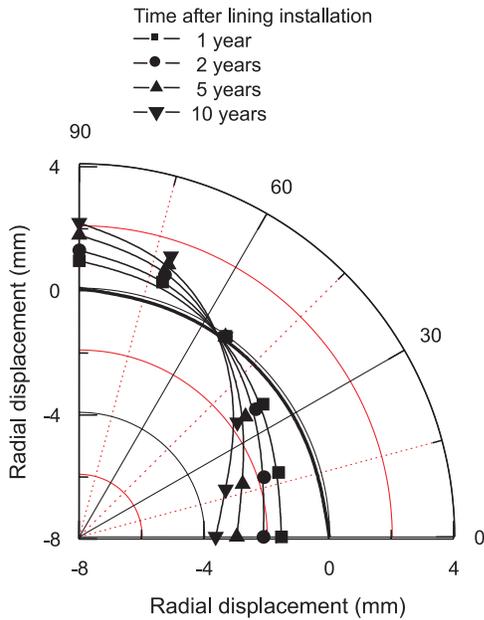
increases with time. The tangential stress is zero at an angular distance $\theta \approx 30°$. The tensile ($f_t = 3.5$ MPa) and compressive ($f_c = 35$ MPa) strengths of the unreinforced concrete lining are also plotted in Fig. 5. As shown, the tensile stress at the springline exceeds the tensile strength of concrete after 2 years and results in tensile cracks at this section. Lo and Yuen (1981) observe that cracking first occurs between CH 135+00 and CH 138+00 at the TBM section between two and two and a half years. The numerical results are therefore consistent with field observations. The zone of tensile cracking increases with time. When the tensile stress exceeds f_t, cracks form in the concrete lining, and the load should be redistributed to the remaining section of the lin-

Fig. 7. Effect of K_0 and t_l on lining stress 10 years after lining installation, Heart Lake tunnel.
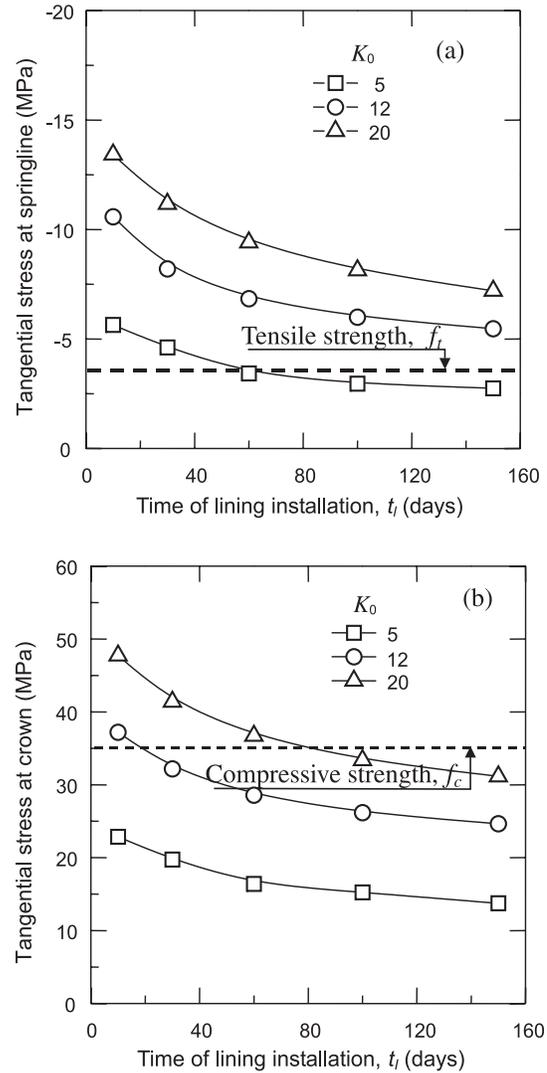
ing. The post-crushing mechanism is not considered in this analysis, however. Figure 5 also shows that the maximum compressive stress (at the crown) after 2 years is well below the compressive strength of concrete. In summary, lining damage begins with tensile cracks at the springline. Similar behaviour has been predicted and observed in the field (Lo and Yuen 1981). This analysis provides further confirmation that the tangential stress at the inner surface of the lining at the springline is crucial for the design of a tunnel in swelling rock.

The radial deformation of the tunnel with time is shown in Fig. 6. The springline moves inward with time while the crown moves upward. The reduction in horizontal tunnel diameter and increase in vertical diameter are observed at several sections since construction of this tunnel.

Effects of t_l and K_0

Figures 7a and 7b show the effects of time lapse (t_l) before lining installation. The tangential stresses at the inner face of the lining at the springline and crown 10 years after lining installation are calculated for three different values of

Fig. 8. Longitudinal profile of Darlington cold-water intake tunnel (after Lo and Lukajic 1984).
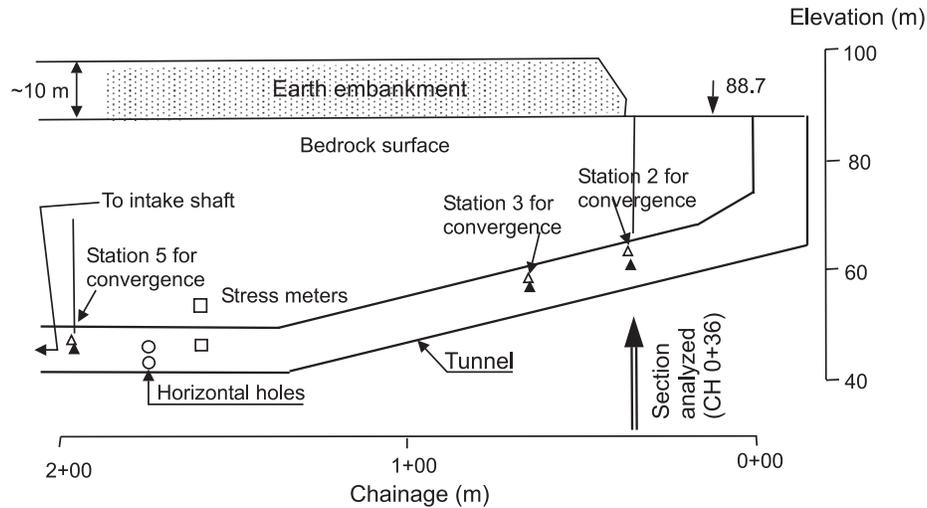
Fig. 9. Convergence and movement of anchored points at springline, Darlington cold-water intake tunnel.

Fig. 10. Finite element mesh used in simulation of Darlington cold-water intake tunnel.
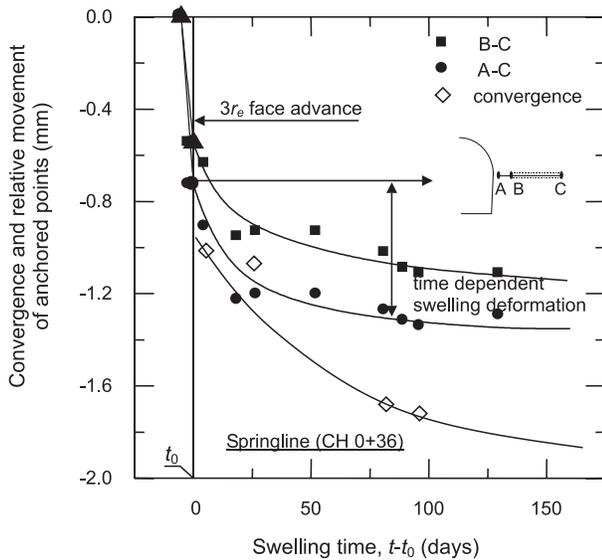
K_0 (5, 12, and 20). The elapsed time between the excavation and the installation of the lining varies from 10 to 150 days (Lo et al. 1979). These figures show that the tangential stress decreases with an increase in t_l for a given value of K_0. On the other hand, the tangential stress increases with an increase in K_0 for the same value of t_l. This trend is similar to that of the previous closed-form solutions (Lo and Yuen 1981; Lo and Hefny 1996). If t_l is less for a large value of K_0 (e.g., t_l = 10 days and K_0 = 20), the lining stresses at the crown and springline exceed the compressive and tensile strengths of concrete, respectively, after 10 years. Figure 7a shows that the formation of cracks at the springline after 10 years is possible in this tunnel if K_0 is relatively large ($K_0 > 6$), even if the lining is installed 150 days after the excavation. A similar response is observed in the field. As it is not possible to leave the tunnel unlined for a long period of time after the excavation, the use of crushable material between the excavated rock surface and the lining, as suggested by Lo and Yuen (1981), could prevent lining damage.

Darlington cold-water intake tunnel

The Darlington Generating Station is a nuclear power generating station located 60 km east of Toronto on the shore of Lake Ontario. A D-shaped cold-water intake tunnel of 8 m span and 925 m length has been constructed in horizontally bedded Lindsay limestone with thin shaly interbeds. The longitudinal profile of the tunnel is shown in Fig. 8. Lo and Lukajic (1984) report the deformation of the tunnel measured at different sections using extensometers.

Typical extensometer readings are shown in Fig. 9 and are obtained from the extensometers at CH 0+36 (Fig. 8) along the springline. The relative displacement is less for extensometer B–C than for extensometer A–C (see inset to Fig. 9). The convergence along the springline is also shown in Fig. 9. The rapid initial inward movement is the elastic deformation that results from the excavation. The movement

Fig. 11. Initial stresses in the horizontal plane at the Darlington Generating Station site.
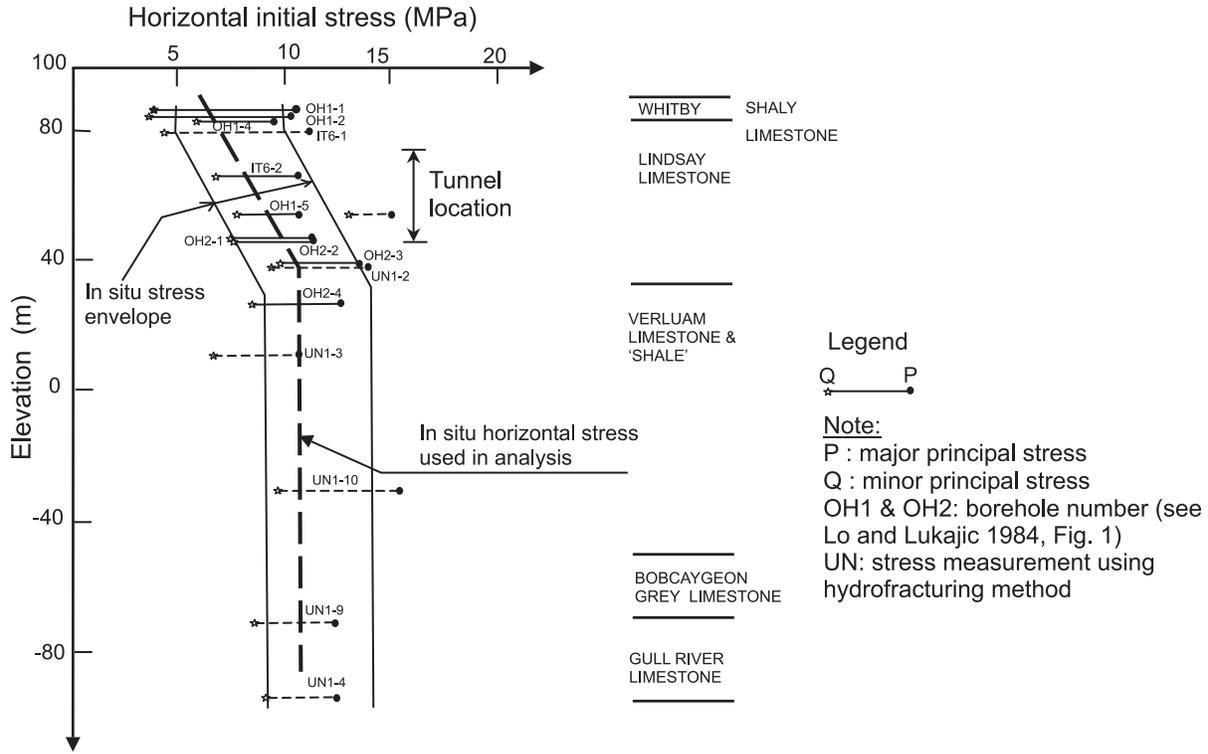
continues with time at a slower rate because of the swelling of the rock.

Results of numerical analysis

Figure 10 shows the dimensions of the tunnel section at CH 0+36 (Fig. 8) and the finite element mesh used in the analyses. The properties of the rock are obtained from previous studies (Lo 1983; Lo and Lukajic 1984) and are listed in Table 1. In situ vertical stress is the overburden pressure, and the in situ horizontal stresses are obtained from the field stress measurements. The in situ horizontal stress increases linearly to elevation 40 m and is constant below this depth (Fig. 11). Elastic finite element analysis performed for this tunnel provides results that are compared with field measurements during construction (Lo and Lukajic 1984). Good agreement is obtained and validates the proper selection of elastic parameters, boundary conditions, and mesh size for the analysis. The relief of initial stress is a necessary condition for swelling of this rock. Elastic analyses of this section show that the relief of initial stress mainly occurs in the Lindsay Formation, and therefore the deformation is governed by the properties of rock in this layer. The properties of this formation have been obtained form laboratory test results (Lo 1983; Lo and Lukajic 1984). The average values of critical stress and pseudo-Poisson's ratio have been used in the analysis.

Time-dependent swelling deformation

Subtracting the convergence of the tunnel at $3r_e$ (Fig. 9), which is treated as purely elastic deformation, the time-dependent convergence of the tunnel is calculated. The time-dependent convergence of the unlined tunnel at the springline ($\delta_{(s)}$) at CH 0+36 (Fig. 8) is shown in Fig. 12. The

predicted time-dependent convergence is also plotted in this figure. The inset to Fig. 12 shows the prediction of the present model in large scale.

The convergence of the tunnel is also calculated using the closed-form solution developed by Yuen (1979). Although the measured swelling potentials are anisotropic, a set of isotropic time-dependent parameters is required for this closed-form solution. The time-dependent parameters are obtained from the best-fitted curve for a given swelling potential. Figure 12 also shows the prediction of the closed-form solution using two swelling potentials that have been used in the present finite element analysis (see Table 1). The closed-form solution overpredicts the swelling deformation, even with the minimum value of free swelling potential ($m_{i(0)} = 0.025\%$). Lo et al. (1984) attributed the possibility of higher shale content in laboratory test specimens for this overprediction, since the most shaly portion was purposely chosen for testing to be used in design analysis. This analysis shows, however, that the reduction of swelling by three-dimensional stresses which was not considered in the closed-form solutions is also the cause of this overprediction.

Figure 13 shows the development of tangential stress at the inner surface of the lining 100 years after the time of installation. A small amount of tensile stress has developed near the springline and invert because of the swelling of rock. On the other hand, compressive stresses developed at the crown and at the corner of the rectangular section. The maximum compressive stress develops at the corner of the flat bottom. However, these tensile and compressive stresses are well below the tensile (~3.5 MPa) and compressive (~35 MPa) strengths of concrete, respectively. In other words, no crack formation in the concrete lining is pre-

Fig. 12. Predicted and measured convergence of Darlington cold-water intake tunnel. Inward movement is negative.
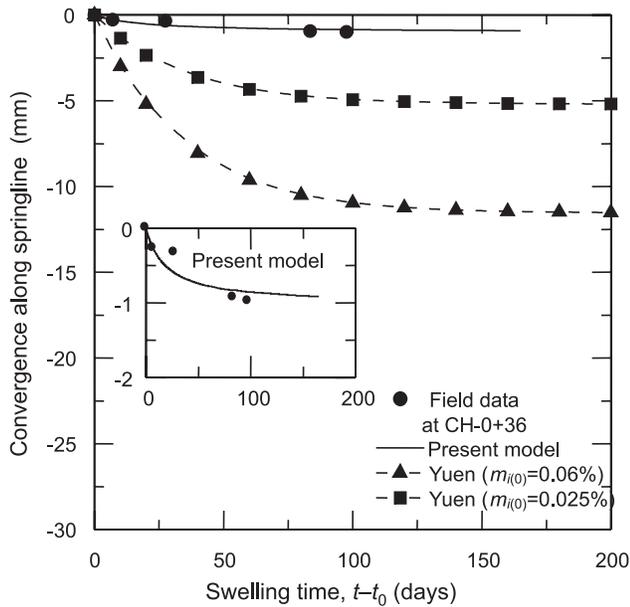
Fig. 13. Predicted tangential stress (in MPa) at the inner face of the lining, 100 years after lining installation (Darlington cold-water intake tunnel; positive compression, negative tension).
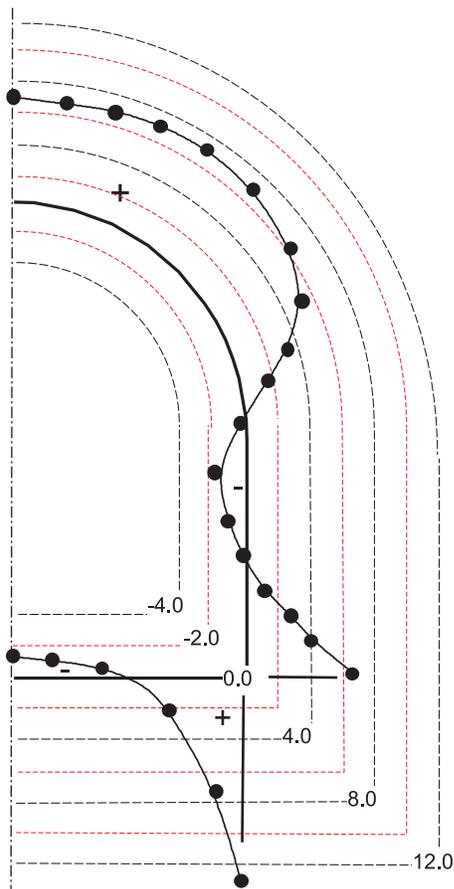
dicted for this tunnel, and a similar response is observed in the field.

Conclusions

Time-dependent swelling deformation is an important issue in the design of underground structures in shaly rocks in southern Ontario. Laboratory test results show that the swelling is three-dimensionally stress dependent. Two rheological models (Lo and Yuen 1981; Lo and Hefny 1996) are available in the literature for time-dependent swelling of these shales, although the three-dimensional stress effects are not examined in these studies. The constitutive model discussed in this paper takes into account the three-dimensional stress effects and long-term swelling with anisotropic swelling potentials. The stress effect is modelled using the pseudo-Poisson's ratio.

A numerical algorithm is developed to implement the model in a finite element program. The model is used to analyze the swelling effects on the Heart Lake storm sewer tunnel and the Darlington cold-water intake tunnel.

The numerical analysis shows that the maximum tensile stress develops at the inner face of the lining near the springline. It can produce tensile cracks in the concrete lining, as observed in the Heart Lake storm sewer tunnel. The tensile stress at this location is critical for design. The lining stress depends on the in situ stress ratio (K_0) and the elapsed time before the installation of the lining (t_l). A high value of K_0 with a low value of t_l results in higher tensile stress. Lo and Yuen (1981) previously reached similar conclusions, which are further confirmed in this study when considering three-dimensional stress effects.

The tunnel converges with time at the springline. The convergence of the Darlington cold-water intake tunnel measured in the field is compared with theoretical predictions. The present model agrees with field measurements of deformation, whereas the closed-form solution overpredicts the magnitude.

Although the present model provides better prediction, the closed-form solutions give a quick estimation of swelling effects on a tunnel. The parameters (μ, σ_c) required for the present model can be obtained directly from modified swell tests (Hawlader et al. 2003). For design, a choice between the present numerical model and closed-form solutions depends on the nature of the project, the completeness of the rock parameters available, and the geological conditions. It would be expedient to use the closed-form solutions (Lo and Yuen 1981; Lo and Hefny 1996) for preliminary design consideration and the present method to examine the selected sections to finalize the design. For underground structures in highly swelling rocks, the present model could significantly facilitate design measures that are to be adopted.

Acknowledgements

References

Carter, J.P., and Balaam, N.P. 1990. AFENA — A general finite element algorithm: users manual. School of Civil and Mining Engineering, University of Sydney, Sydney, NSW, Australia.

Einstein, H.H., Bischoff, N., and Hofmann, E. 1972. Behaviour of invert slabs in swelling shale. *In* Proceedings of the International Symposium on Underground Openings, Lucerne, Switzerland. Schweiz, Zurich. pp. 296–319.

Grob, H. 1972. Schwelldruc im Belchentunnel. *In* Proceedings of the International Symposium on Underground Openings, Lucerne, Switzerland. Schweiz, Zurich. pp. 99–119.

Hawlader, B.C., Lee, Y.N., and Lo, K.Y. 2003. Three-dimensional stress effects on time-dependent swelling behaviour of shaly rocks. Canadian Geotechnical Journal, **40**: 501–511.

ISRM Commission on Swelling Rock. 1994. Comments and recommendations on design and analysis procedures for structures in argillaceous swelling rock. International Journal of Rock Mechanics and Mining Sciences and Geomechanics Abstracts, **31**: 537–546.

Lee, Y.N. 1988. Stress–strain–time relationship of Queenston shale. Ph.D. thesis, University of Western Ontario, London, Ont.

Lee, C.F., and Lo, K.Y. 1976. Rock squeeze study of two deep excavations at Niagara Falls. *In* Rock Engineering: Proceedings of the ASCE Specialty Conference for Foundations and Slopes, Boulder, Colo., 15–18 August 1976. ASCE, New York. pp. 116–140.

Lee, Y.N., and Lo, K.Y. 1993. The swelling mechanism of Queenston shale. Canadian Tunnelling, pp. 75–97.

Lo, K.Y. 1978. Regional distribution of in-situ horizontal stresses in rocks of southern Ontario. Canadian Geotechnical Journal, **15**: 371–381.

Lo, K.Y. 1983. Results of field instrumentation and performance evaluation, C.W. intake tunnel, Darlington G.S. Ontario Hydro Report 83099.

Lo, K.Y. 1986. Advances in design and performance evaluation: keynote address. *In* Recent Advances in Canadian Tunnelling Technology: Proceedings of the 6th Canadian Tunneling Conference, Niagara Falls, Ont., October 1986. *Edited by* K.Y. Lo, C.M.K. Yuen, and J.H.L. Palmer. Tunnelling Association of Canada, Toronto, Ont. pp. 5–46.

Lo, K.Y., and Hefny, A. 1996. Design of tunnels in rock with long-term time-dependent and nonlinearly stress-dependent deformation. Canadian Tunnelling, pp. 179–214.

Lo, K.Y., and Lee, Y.N. 1990. Time-dependent deformation behaviour of Queenston shale. Canadian Geotechnical Journal, **27**: 461–471.

Lo, K.Y., and Lukajic, B. 1984. Predicted and measured stresses and displacements around the Darlington intake tunnel. Canadian Geotechnical Journal, **21**: 147–165.

Lo, K.Y., and Yuen, C.M.K. 1981. Design of tunnel lining in rock for long-term time effects. Canadian Geotechnical Journal, **18**: 24–39.

Lo, K.Y., Wai, R.S.C., Palmer, J.H.L., and Quigley, R.M. 1978. Time-dependent deformation of shaly rock in southern Ontario. Canadian Geotechnical Journal, **15**: 537–547.

Lo, K.Y., Devata, M., and Yuen, C.M.K. 1979. Performance of a shallow tunnel in a shaly rock with high horizontal stresses. *In* Tunnelling '79: Proceedings of the 2nd International Symposium on Tunnelling. *Edited by* M.J. Jones. Institution of Mining and Metallurgy, London, UK. pp. 1–12.

Lo, K.Y., Lukajic, B., and Ogawa, T. 1984. Interpretation of stress–displacement measurements. *In* Tunnelling in Soil and Rock: Proceedings of Two Sessions at Geotech'84, Atlanta, Ga., 14–16 May 1984. ASCE, New York. pp. 128–155.

Lo, K.Y., Cooke, B.H., and Dunbar, D.D. 1986. Design of buried structures in squeezing rock in Toronto, Canada. *In* Proceedings of the 6th Canadian Tunnelling Conference, Niagara Falls, Ont. Tunnelling Association of Canada, Toronto, Ont. pp. 159–198.

Trow, W.A., and Lo, K.Y. 1989. Horizontal displacements induced by rock excavation: Scotia Plaza, Toronto. Canadian Geotechnical Journal, **26**: 114–121.

Wittke, W., and Pierau, B. 1979. Fundamentals for the design and construction of tunnels in swelling rock. *In* Proceedings of the 4th International Congress on Rock Mechanics, Montreux, Switzerland, 2–8 September 1979. International Society of Rock Mechanics, A.A. Balkema, Rotterdam. Vol. 2, pp. 719–729.

Yuen, C.M.K. 1979. Rock–structure time interaction in lined circular tunnels in high horizontal stress field. Ph.D. thesis, Faculty of Engineering Science, University of Western Ontario, London, Ont.

Zienkiewicz, O.C., and Cormeau, I.C. 1974. Visco-plasticity–plasticity and creep in elastic solids — a unified numerical solution approach. International Journal for Numerical Methods in Engineering, **8**: 821–845.

Zienkiewicz, O.C., and Taylor, R.L. 1990. Finite element method. Vol. 2. 4th ed. McGraw-Hill, New York.

List of symbols

d_c thickness of concrete lining

E elastic modulus

f_c compressive strength of concrete

f_t tensile strength of concrete

K_0 initial stress ratio = σ_{x0}/σ_{y0}

m_i swelling potential in ith direction under three-dimensional stress

$m_{i(0)}$ free swelling potential in ith direction

r radial distance

r_1, r_2 radius of excavation

r_e equivalent radius of tunnel

R_{ij} reduction ratios

t time

t' time after lining installation

t_0 reference time at which swelling begins

t_l time of lining installation

x, y horizontal and vertical axes

δ_{ij} Kronecker delta

ε_i^s swelling strain in ith direction

μ_{ij} pseudo-Poisson's ratios

ν Poisson's ratio

σ_p principal stress

σ_c critical stress after which no swelling occurs

σ_{th} threshold stress below which there is no stress effect on swelling

σ_{x0}, σ_{y0} horizontal and vertical stress

θ angular distance

Ω volume of the body

Vectors and matrices

a displacement vector

B strain–displacement matrix

B^T transpose of matrix B

D elastic moduli matrix

F^* pseudo-load vector

F_{ext}^{n} external force vector at nth time step

F_{int}^{n} internal force vector at nth time step

$\mathbf{K}$ stiffness matrix

$\boldsymbol{m}$ swelling potential vector

$\boldsymbol{m}_{\sigma_p}$ swelling potential in the principal stress direction

$\boldsymbol{\alpha}_{pi}$ rotation of the principal stress vector

$\boldsymbol{\varepsilon}$ strain vector

$\boldsymbol{\varepsilon}^{s}$ swelling strain vector

$\dot{\boldsymbol{\varepsilon}}$ total strain rate vector

$\dot{\boldsymbol{\varepsilon}}^{e}$ elastic strain rate vector

$\dot{\boldsymbol{\varepsilon}}^{s}$ swelling strain rate vector

$\boldsymbol{\sigma}$ stress vector

$\dot{\boldsymbol{\sigma}}$ stress rate vector

$\boldsymbol{\sigma}_{p}$ principal stress vector